Heliyon 6 (2020) e05714

Contents lists available at ScienceDirect

Heliyon

journal homepage: www.cell.com/heliyon

Research article

Effect of the interaction between ribosomal protein L10a and insulin receptor on carbohydrate metabolism

Netnapa Chaichanit [a], Uraipan Saetan [a], Monwadee Wonglapsuwan [a,b], Wilaiwan Chotigeat [a,b,*]

[a] Department of Molecular Biotechnology and Bioinformatics, Faculty of Science, Prince of Songkla University, Hatyai, Songkhla, 90112, Thailand
[b] Center for Genomics and Bioinformatics Research, Faculty of Science, Prince of Songkla University, Hatyai, Songkhla, 90112, Thailand

ARTICLE INFO

Keywords:
Ribosomal protein L10a
Insulin receptor
Diabetes
Insulin resistance
Glucose metabolism
Food science
Agricultural science
Environmental science
Biological sciences
Health sciences

ABSTRACT

The number of patients with insulin-resistant diabetes has significantly increased. Thus, alternative insulin mimetics are required for such patients. Some evidences indicate that ribosomal protein L10a (RpL10a) is involved in the insulin pathway. In addition, we previously demonstrated that recombinant RpL10a from *Fenneropenaeus merguiensis* (*Fm*-RpL10a) could stimulate cell proliferation and trehalose metabolism in RpL10a–over-expressing flies by inducing *insulin receptor* (*InR*) expression and some insulin signaling mediators phosphorylation. In this study, we investigated the *in silico* binding between *Fm*-RpL10a and InR. The results indicated that *Fm*-RpL10a bound to InR at residues 635–640 and 697–702 of the FnIII2 domain. This binding was confirmed using a pull-down and immunofluorescence assay. Further analysis indicated that *Fm*-RpL10a could stimulate glucose utilisation by insulin-resistant cells (IRCs) and healthy cells. Additionally, *Fm*-RpL10a at a low concentration (1 μg/ml) altered some glucose metabolism-related genes expression in *Fm*-RpL10a treated IRCs. The qRT-PCR result revealed the up-regulation of *Hk1*, which encode key enzymes in glycolysis. Conversely, the expression of *G6pc3*, which participates in gluconeogenesis, was down-regulated. Overall, the results suggest that *Fm*-RpL10a can alleviate insulin resistance by stimulating insulin signaling via the FnIII2 domain of InR and activate glycolysis. Therefore, *Fm*-RpL10a may be a candidate insulin mimetic for the treatment of diabetes.

1. Introduction

The insulin signaling pathway is a biochemical pathway involved in many biological processes such as glucose homeostasis, proliferation and apoptosis. The signal transduction in this pathway consists of an autophosphorylation mechanism that acts as a signal throughout the cell after the insulin receptor (InR) is activated via binding to insulin or other ligands such as an insulin-like growth factor. InR, a transmembrane receptor protein, belongs to the superfamily of receptor tyrosine kinases. The structure of InR includes two extracellular α-subunits containing the insulin binding domain and two transmembrane β-subunits exhibiting ligand-activated tyrosine kinase activity (Belfiore et al., 2009; Seino and Bell, 1989). InR consists of two ligand-binding sites, one of which consists of L1 and αCT domains. The other ligand-binding site consists of FnIII1 and FnIII2 domains (Ward and Lawrence, 2009). It is well known that insulin plays an essential role in controlling blood glucose levels. The insulin activates the pathway via binding to the InR extracellular α-subunit, leading to autophosphorylation-mediated signal transduction that induces glucose uptake for metabolism and storage. Insulin resistance is caused by malfunction of InR or signal transduction, resulting in abnormal glucose metabolism and leading to type 2 diabetes mellitus (T2DM) (Campbell, 2009). Contrarily, type 1 diabetes mellitus (T1DM) caused by the beta cells were destroyed by the autoimmune response leading to abnormal insulin production in the pancreas (Bluestone et al., 2010). Therefore, insulin replacement therapy is widely used to treat patients with T1DM and some patients with T2DM. However, many reports suggested that recombinant insulin, its analogues and insulin mimetic can be used to treat patients with diabetes (Babu et al., 2020; Moura et al., 2020; Qiang et al., 2014; Xie et al., 2020).

Several ribosomal proteins involved in the insulin pathway. Ribosomal protein S26 (RpS26) is highly expressed in the pancreas and islets of Langerhans and directly linked to many genes associated with T1DM such as histocompatibility 2, class II antigen *E beta* (*H2-Eb1*), a T1DM susceptibility gene (Schadt et al., 2008). The ribosomal protein S6 kinase 1 (S6K1), a component of insulin signaling transduction, negatively regulates insulin receptor substrate 1 (IRS1) (Yoon, 2017). Studies in mice illustrated that the absence of S6K1 results in mild glucose intolerance and reduced circulating insulin levels (Pende et al., 2000). In

* Corresponding author.
E-mail address: wilaiwan58@hotmail.com (W. Chotigeat).

https://doi.org/10.1016/j.heliyon.2020.e05714
Received 18 July 2020; Received in revised form 12 October 2020; Accepted 9 December 2020
2405-8440/© 2020 The Author(s). Published by Elsevier Ltd. This is an open access article under the CC BY-NC-ND license (http://creativecommons.org/licenses/by-nc-nd/4.0/).

addition, S6K1 might be involved in nutrient overload-induced insulin resistance (Tremblay et al., 2005; Um et al., 2004).

Ribosomal protein L10a (RpL10a) is a component protein of the large ribosomal subunit. RpL10a was reported to be involved in cell proliferation, embryogenesis, organogenesis (Balcer-Kubiczek et al., 1997; Fisicaro et al., 1995) and maturation in shrimp ovaries (Palasin et al., 2014; Wonglapsuwan et al, 2010, 2011). Moreover, some studies described the relationship between RpL10a and InR (Pritchett and McCall, 2012; Wonglapsuwan et al., 2011) and the up-regulation of both *RpL10a* and *InR* during ovarian maturation was reported (Saetan et al., 2016). Additionally, our previous study indicated that *Fm*-RpL10a could stimulate cell proliferation and increase trehalose metabolism in RpL10a-–over-expressing flies by inducing the expression of InR (Chaichanit et al., 2018) and phosphorylation of Protein kinase B (Akt) and Forkhead box protein O (FOXO), a member of insulin signaling mediator, in RpL10a–over-expressing flies. These results reveal that *Fm*-RpL10a is related to InR and the insulin pathway, which affects cell proliferation and metabolism.

In the present study, the *Fm*-RpL10a as an insulin mimetic was shown. We showed the evidences that *Fm*-RpL10a interacts with InR and the effects of their binding on downstream pathways, especially the insulin signaling pathway. Therefore, insulin-resistant cells (IRCs) were generated and the usage of glucose by the cells was occurred after treatment with the recombinant *Fm*-His-RpL10a protein. Besides, the expression of the rate limiting enzymes in glycolysis and gluconeogenesis pathway of the *Fm*-His-RpL10a–treated IRCs was carried out to confirm the glucose utilisation through qRT-PCR.

2. Materials and methods

2.1. In silico binding of Fm-RpL10a and InR

The structure of RpL10a protein was taken from the NCBI database. The accession number is ACU52718. The 3D structure was modelled on the basis of template ID 6gz3.76.A with 71.43% identity. The 3D structure of InR was taken from the RCSB Protein Data Bank (PDB). The ID of human InR is 3LOH from X-ray diffraction with a resolution of 3.8 Å. Then, protein–protein docking was performed using the PIPER programme on the ClusPro 2.0 server. *Fm*-RpL10a was used as a ligand, whereas InR served as a receptor. The model with the largest cluster and high lowest energy scores was selected. After that, the selected model was elucidated using the PyMol programme. The scores of the interaction, including balanced, electrostatic-favoured, hydrophobic-favoured and van der Waals interactions, were determined using the same methods. The insulin model was derived from PDB entry 3e7y produced from X-ray diffraction with a resolution of 1.6 Å.

2.2. Determination of the interaction between Fm-RpL10a and InR using the pull-down assay

To confirm the binding between RpL10a and InR using the pull-down assay, the target binding site (FnIII2 domain) of InR from Chinese hamster ovary (CHO–S) cells (Gibco, USA) was produced. First, the InR protein sequences from Chinese hamsters (GenBank: Accession No. XP_016833794) and humans (UniProtKB: P06213) were compared using ClustalX 2.0 to determine the gene identity. The conserved domain of these protein sequences was predicted using ScanProsite tools to locate the binding site. Then, the target binding site was cloned into the pGEX-4T-1 (GE Healthcare, Chicago, IL, USA) expression vector as a bait protein in the pull-down assay. For the prey protein, the full-length of *Fm*-RpL10a in a pET-28a (+) (Novagen, Madison, WI, USA) expression vector was obtained from a previous study (Wonglapsuwan et al., 2010).

2.3. Cloning of InR-FnIII2

Total RNA was isolated from CHO–S cells using TRIzol reagent (Invitrogen, Carlsbad, CA, USA) according to the manufacturer's protocol. Two micrograms of total RNA were synthesised into cDNA using AMV Reverse Transcriptase (Promega, Madison, WI, USA). The target binding site, namely the FnIII2 domain of *InR*, was amplified from CHO–S cell cDNA using an *InR* forward primer carrying a *Sal*I restriction site (5′-TTA GTC GAC TGC ACC TGT ACC CCG GAG AG-3′) and an *InR* reverse primer featuring a *Not*I restriction site (5′-CAT GCG GCC GCT CAG ACA GAA GGG TTA GTG GCA TC-3′). The PCR fragments were cloned into a pGEM-T Easy cloning vector (Promega) and transformed into *Escherichia coli* Top 10 F′ competent cells. The sequence analysis was performed using an ABI PRISM® 310 Genetic Analyzer. The nucleotide sequence was translated into the amino acid sequence using the translate tool of ExPASy. The predicted amino acid sequence was aligned with the Chinese hamster and human InR protein sequences to determine the identity. The molecular mass and pI of InR-FnIII2 protein were computed by the ProtParam tool of ExPASy.

2.4. Expression and purification of the recombinant GST-InR-FnIII2 gene

The recombinant pGEM-InR-FnIII2 gene was digested using *Sal*I and *Not*I (Promega) restriction enzymes and ligated to the pGEX-4T-1 expression vector before transformation in *E. coli* BL21 (DE3) competent cells. The recombinant GST-InR-FnIII2 protein was produced using a single colony of *E. coli* BL21 (DE3) carrying the recombinant *pGEX-InR-FnIII2* plasmid. A colony was inoculated in 1 ml of LB broth containing 100 μg/ml ampicillin and grown overnight at 37 °C with agitation at 180 rpm. The overnight culture of 100 μl was transferred to 10 ml of LB broth containing 100 μg/ml ampicillin and grown at 37 °C with agitation at 180 rpm until the optical density (OD) at 600 nm reached 0.5–0.8. Recombinant GST-InR-FnIII2 protein expression was then induced by the addition of 0.1 mM isopropyl-1-thio-β-D-galactosidase (IPTG) to the cell culture and grown at 37 °C with agitation at 180 rpm for 4 h. After the induction, the bacterial cells were harvested and re-suspended in phosphate-buffered saline (PBS, 140 mM NaCl, 2.7 mM KCl, 10 mM Na_2HPO_4, 1.8 mM KH_2PO_4, pH 7.3). The cell suspension was sonicated and centrifuged at 12,000 × *g* for 10 min. The supernatant was collected as a soluble protein fraction. Then, the soluble GST-InR-FnIII2 protein was purified via incubation with Glutathione Sepharose® 4 Fast Flow (GE Healthcare) overnight at 4 °C. The protein mixer was centrifuged at 500 × *g* for 5 min, and the excess protein was removed. The protein mixture was washed five times with PBS to remove unbound protein. Then, the GST-InR-FnIII2 protein was eluted with elution buffer (50 mM Tris-HCl, 10 mM reduced glutathione, pH 8.0). The purified GST-InR-FnIII2 protein was finally confirmed via SDS-PAGE.

The recombinant *Fm*-His-RpL10a protein was obtained from a previous study (Wonglapsuwan et al., 2010). A single colony of *E. coli* BL 21 (DE3) harbouring the pET-*Fm*-RpL10a plasmid was inoculated in 30 ml of LB broth containing 30 μg/ml kanamycin and grown overnight at 37 °C with rotating at 180 rpm. Subsequently, the overnight culture was transferred to 300 ml of LB broth containing 30 μg/ml kanamycin and grown at 28 °C with shaking at 180 rpm until the OD at 600 nm reached 0.5–0.7. Then, recombinant *Fm*-His-RpL10a protein expression was induced by adding 1.0 mM IPTG to the cell culture, and the cells were grown at 18 °C with agitation at 120 rpm for 16–18 h. The cells were then harvested by centrifugation at 4000 × g for 20 min, and the cell pellet were solubilised in 10 ml of lysis buffer (50 mM NaH_2PO_4, 300 mM NaCl, 10 mM Tris-HCl, pH 8.0). The cell suspension was sonicated, and the supernatant was collected by centrifugation at 10,000 × g for 20 min. The recombinant *Fm*-His-RpL10a protein was filtered using a 0.2-μm

filter, applied to a His-Trap FF column (GE Healthcare Bio-Sciences, Sweden) and examined using the ÄKTA prime chromatography system following the manufacturer's instructions (GE Healthcare Bio-Sciences). The purity of the purified *Fm*-His-RpL10a protein was dialysed against the dialysis buffer (350 mM NaCl, 50 mM NaH_2PO_4, pH 7.4), and the purity of the *Fm*-His-RpL10a protein was determined by SDS-PAGE.

2.5. Pull-down assay

To determine the physical interaction between RpL10a and InR using the GST pull-down assay, 10 μg of the GST-InR-FnIII2 protein in 200 μl of dialysis buffer were incubated overnight with 20 μl of a 50% slurry of Glutathione Sepharose 4 Fast Flow at 4 °C with end-over-end mixing. The protein mixture was then centrifuged at 500 × *g* for 5 min, and the excess protein was removed. The mixture was washed four times with dialysis buffer to remove unbound protein. Then, 10 μg of the recombinant *Fm*-His-RpL10a protein in 200 μl of dialysis buffer were added to the pre-incubated GST-InR-FnIII2 with Glutathione Sepharose 4 Fast Flow beads and then incubated again overnight at 4 °C with end-over-end mixing. Excess protein was removed, and the mixture was washed four times with dialysis buffer. Then, 20 μl of SDS sample loading dye were added to the protein–protein interaction complex mixture, and the mixture was boiled for 5 min followed by spinning at 13,000 × *g* for 10 min to precipitate the Glutathione Sepharose beads. The supernatant containing the protein–protein interaction complex was separated on a 12% SDS-PAGE gel and transferred to nitrocellulose membranes. The membranes were blocked with PBS containing 0.1% Tween 20 (PBST) buffer containing 5% w/v BSA for 4 h before incubation with primary antibodies for 2 h. A mouse monoclonal RpL10a antibody (Abcam, Cambridge, UK) and a goat polyclonal GST antibody (GE Healthcare Bio-Sciences, Sweden) were diluted 1:3000. The membranes were washed three times with PBST and incubated with a 1:5000 dilution of rabbit anti-mouse AP (Santa Cruz, CA) and rabbit anti-goat AP (Invitrogen, Carlsbad, CA, USA) antibodies for 2 h. The membranes were then washed with PBST and then exposed to nitro blue tetrazolium chloride/5-bromo-4-chloro-3-indolyl phosphate, toluidine salt (NBT/BDIP) (Roche, Germany). GST incubated with *Fm*-His-RpL10a and GST-InR-FnIII2 was used as a control.

2.6. Confirmation of the interaction between RpL10a and InR using an immunofluorescence assay

CHO–S cells were grown on glass coverslips in a 6-well plate containing Dulbecco's Modified Eagle's Medium (DMEM, Gibco) with 10% heat-inactivated fetal bovine serum (FBS, Gibco) and 1% antibiotic–antimycotic (Gibco) for 18 h at 37 °C in an atmosphere of 5% CO_2. After 18 h of culturing, the medium was changed to DMEM containing 3 μg/ml *Fm*-His-RpL10a, and cells were incubated for 6 h at 37 °C in an atmosphere of 5% CO_2. Then, the incubated cells were washed three times with PBS. The cells were fixed with cool methanol at room temperature for 5 min and then washed three times with PBS. After washing, the fixed cells were blocked with blocking buffer (PBS containing 0.1% Triton X-100, 1% BSA and 22.52 mg/ml glycine) for 30 min and were incubated with a 1:1000 dilution of rabbit polyclonal anti-insulin Rβ antibody (Santa Cruz) and mouse monoclonal anti-6X His tag® antibody (Thermo Fisher Scientific, Waltham, MA, USA) for 3 h. After incubation, the primary antibody was removed, and cells were washed three times with PBS. Cells were subsequently incubated with a 1:5000 dilution of goat anti-rabbit IgG conjugated with rhodamine and goat anti-mouse IgG conjugated with FITC (Santa Cruz) for 1 h in the dark. The antibody solution was removed, and cells were washed with PBS. The cells were stained with DAPI solution (Thermo Fisher Scientific, Waltham, MA, USA) for 5 min in the dark and then washed with PBS before mounting. The stained cells were observed on an Olympus BX51 microscope.

2.7. Induction of IRCs

CHO–S cells were seeded 3.5 × 10^5 cells/well in 12-well plate and maintained in DMEM which contains 25 mM of glucose supplemented with 10% FBS, and 1% antibiotic–antimycotic for 18 h at 37 °C in an atmosphere of 5% CO_2. IRCs were induced in DMEM under three conditions, including supplemented with glucose to final concentration 50 mM, high insulin (100 nM) and high glucose plus insulin (50 mM glucose and 100 nM insulin). Briefly, the seeded cells were cultured with fresh serum-free DMEM containing additional glucose and/or insulin at 37 °C in a 5% CO_2 atmosphere for 24 h. The cells in DMEM which contains 25 mM of glucose were used as a control. Each condition was performed in triplicate. During 24 h of induction, the character of insulin resistance was determined by collecting the culture medium after 0, 12 and 24 h of induction to measure the glucose consumption rate.

2.8. Fm-RpL10a stimulation for glucose utilisation

After 48 h of insulin resistance induction, IRCs were incubated with fresh serum-free DMEM which contains 25 mM of glucose supplemented with 1, 5 or 15 μg/ml recombinant *Fm*-His-RpL10a protein for 24 h at 37 °C with 5% CO_2. Normally, the pancreas releases more insulin to help glucose enter the cells in insulin resistance condition. Therefore, DMEM (25 mM of glucose) supplemented with 500 nM insulin is a higher concentration than the dose used to induce IRCs (100 nM insulin), was used as a control in this study (Lee et al., 2012). Each group at each time points was performed in triplicate. During stimulation, the medium was collected to measure the glucose consumption rate. After stimulation, the stimulated cells were used for qRT-PCR analysis, whereas untreated cells served as a control.

The medium was collected after 0, 12 and 24 h of *Fm*-His-RpL10a stimulation. The medium glucose levels were then measured at the indicated time points using the anthrone colorimetric assay, as described previously with modification (Van Handel, 1985). The residual sediment cells in collected medium was removed by centrifugation at 13,000 rpm for 10 min, and 2 μl of the medium were transferred to a glass tube containing 198 μl of distilled water (1:100 dilution). The diluted medium was mixed with 1 ml of anthrone reagent, heated at 90–92 °C for 17 min and cooled before measurement of the green colour intensity using the OD at 625 nm. Each sample was examined in triplicate, and the glucose content was calculated directly from a glucose standard curve. The standard glucose was prepared from 1 mg/ml glucose in 25% ethanol. The glucose stock was diluted to 25, 50, 100 and 200 μg/ml. Two hundred microliters of each dilution of standard glucose were mixed with anthrone reagent and analysed as described previously.

2.9. qRT-PCR analysis of glucose metabolism-related gene expression

The expression of Hexokinase (HK) and Phosphofructokinase (PFK) enzyme in glycolysis pathway were selected to check whether the glucose increases glycolysis and goes to TCA cycle after the uptake of glucose into the IRCs. HK which is the rate limiting enzyme in glycolysis (Beutler, 1972; Robey and Hay, 2006) while PFK is the enzyme to prepares the substrate for TCA cycle. In contrast, glucose 6-phosphatase (G6Pase) enzymes is a final step of gluconeogenesis to generate free glucose in blood (Nordlie, 1985). Therefore, the expression of these genes were investigated. First, Total RNA was isolated from IRCs and 1 μg/ml *Fm*-His-RpL10a–treated IRCs using TRIzol reagent according to the manufacturer's instructions. The purity and quantity of isolated RNA were determined by the NanoDrop™ 2000c Spectrophotometers (Thermo Scientific, Waltham, MA, USA) and the integrity of RNA was examined by agarose gel electrophoresis before cDNA synthesis. Two micrograms of total RNA were reverse-transcribed into cDNA using AMV Reverse Transcriptase. Real-time PCR was conducted in a 12.5 μl reaction volume containing 10 ng of cDNA template, 300 nM of specific primers and 6.25 μl of 2× FastStart SYBR Green Master Mix (ABI, CA, USA). All

samples were analysed in triplicate and each samples were performed by Real-time PCR in triplicate. The gene expression level of *Fm*-His-RpL10a treated IRCs was compared with untreated IRCs gene expression. The fold changes in glucose metabolism-related gene expression were determined using the $2^{-\Delta\Delta CT}$ method (Livak and Schmittgen, 2001). Gene expression was normalised to that of the β-actin gene. The primer sequences for qRT-PCR are shown in Table 1.

2.10. Statistical analysis

Statistical analysis was performed using SPSS version 15.0 software (SPSS Inc., Chicago, IL, USA). In the glucose utilisation by cells, three separated samples were tested using two-way ANOVA with Tukey's multiple comparison test and independent-samples *t*-test was used to compare the treated group with untreated group at the same time point. Independent-samples *t*-test was used for comparing the expression levels of *Hk1*, *Pfk1*, and *G6pc3* genes. The data are presented as the mean ± SD. *, $P < 0.05$ was considered statistically significant.

2.11. Ethic statement

All experiments have been approved by the Ethics Committee for animal care and use, Prince of Songkla University.

3. Results

3.1. Binding of Fm-RpL10a to InR at a different binding site than insulin

The 3D structures of RpL10a and InR were downloaded from the PDB and docked using ClusPro 2.0 to predict whether RpL10a interacts with InR. Interestingly, the software predicted with high scores that RpL10a could bind to InR (Figure 1c). The lowest energies of balanced, electrostatic-favoured, hydrophobic-favoured, and van der Waals interactions were −958.1, −1010.7, −1174.8, and −361.3, respectively. We suggest that the interaction of these two proteins may allow RpL10a to initiate the activity of the insulin signaling pathway via InR. We also observed that the site at which RpL10a bound to InR was different from that used by insulin (Figure 1a and 1c). RpL10a interacts at residues 635–640 and 697–702 of InR, which is a part of the FnIII2 domain (Figure 1d and 1e), whereas insulin binds at residues 704–710 (Figure 1b). The lowest energies of the balanced, electrostatic-favoured, hydrophobic-favoured, and van der Waals interactions of insulin-InR binding were −1079.5, −1045.2, −1481.3, and −192.8, respectively.

We performed a GST pull-down assay to confirm whether RpL10a could interact with InR. First, the FnIII2 domain (including residues 635–640 and 697–702) of InR was obtained from CHO–S cells. The InR-FnIII2 cDNA clone consisted of 423 bp translated into 141 amino acid residues with a molecular weight and pI of 16.20 kDa and 4.72, respectively. The RpL10a-binding site as indicated by *in silico* analysis was located at residues 59–64 and 121–126 of the InR-FnIII2 clone. Conversely, the insulin-binding site was located at residues 128–134 of the InR-FnIII2 clone (Figure 2). The InR-FnIII2 protein clone displayed 100 and 98.8% amino acid identities with the *C. griseus* and *H. sapiens* full-length InR proteins, respectively (Figure 3). Although this comparison revealed some amino acid differences between humans and Chinese hamsters, the amino acid sequence at the binding site was 100% identical (Figure 3). Then, the FnIII2 domain of *InR* was cloned into a pGEX expression vector, whereas full-length *Fm-RpL10a* was cloned into a pET-28a (+) expression vector. The GST-InR-FnIII2 and *Fm*-His-RpL10a recombinant proteins were expressed and purified (Figure 4a). As shown in Figure 4b, GST-InR-FnIII2 exhibited an association with *Fm*-His-RpL10a. Notably, no reactive *Fm*-His-RpL10a band was found in the GST panel, indicating that there was no false-positive reaction between GST and *Fm*-His-RpL10a.

Moreover, we also confirmed the interaction of these proteins using an immunohistochemistry assay. CHO–S cells were incubated with *Fm*-His-RpL10a, and binding between *Fm*-His-RpL10a and CHO InR was observed using anti-His and anti-InR antibodies (Figure 5). InR was expressed in the cellular membrane (Figure 5a), whereas *Fm*-His-RpL10a was detected throughout the cells (Figure 5b), indicating that *Fm*-RpL10a could bind with InR (Figure 5d). In the control group, in which no antibody was used, a null fluorescence signal was observed (Figure 5e–h).

3.2. Fm-RpL10a induces glucose utilisation under insulin resistance

We recently reported that *Fm*-RpL10a over-expression in fruit flies decreased whole-body trehalose blood levels in insects by inducing InR expression and activating insulin signaling mediators (Chaichanit et al., 2018). In this study, we investigated whether *Fm*-RpL10a could induce glucose utilisation in IRCs. It's well known that the hyperinsulinemia (Shanik et al., 2008) and hyperglycemia (Buranasin et al., 2018; Nelson et al., 2000) are the risk factors to develop insulin resistance, a condition in which the cells resist insulin stimulation and lead to decrease blood glucose uptake. In this condition, the pancreas release more insulin to help glucose enter the cells. This study, we induced insulin resistance in CHO–S cells under high glucose and/or high insulin conditions. The result indicated that the exposure of CHO–S cells to 50 mM glucose was sufficient to reduce glucose utilisation, indicating insulin resistance (Figure 6a). According to the previous report indicated that high-glucose (50 and 75 mM) delayed wound healing in high glucose-induced cells (Buranasin et al., 2018). Moreover, we also confirmed the induction capability of this condition by extending the duration of induction to 48 h, finding that glucose levels in the culture medium were reduced to approximately 70% of the glucose levels in control medium (the medium with out any cells) (Figure 6b), whereas no difference in the number of cells was noted between the two groups (Figure 6c). Thus, insulin resistance was induced via exposure to 50 mM glucose for 48 h for the next experiment.

IRCs were stimulated with three concentrations of recombinant *Fm*-His-RpL10a, and the glucose content in the culture medium of healthy cells and IRCs was quantified over 24 h of stimulation. The statistical analysis with two-way ANOVA showed that the factors of incubation time, induction condition, and the interaction of two factors affect the

Table 1. Primer sequences for qRT-PCR.

Primer name	Primer sequences (5'to 3′)	PCR product size (bp)	GenBank: Accession No.
Hk1-F	GGA GTG GAT GGG ACG CTC TA	127	XM_027388256.2
Hk1-R	CTT GCC ACT GCC ATC TTC AG		
G6pc3-F	TCT TCT CAG GTG GCA TCT CG	128	XM_003504490.3
G6pc3-R	ACC TGG TGA GGG AAA TGT GC		
Pfk1-F	GAA GGT GGT GGC CTT CAG TC	137	XM_016974718.2
Pfk1-R	CTG CCA TGC TGA TTC GGT AG		
β-Actin-F	GCT ACA GCT TCA CCA CCA CCG	278	AB003910.1
β-Actin-R	GAT GTC CAC GTC RCA CTT CAT		

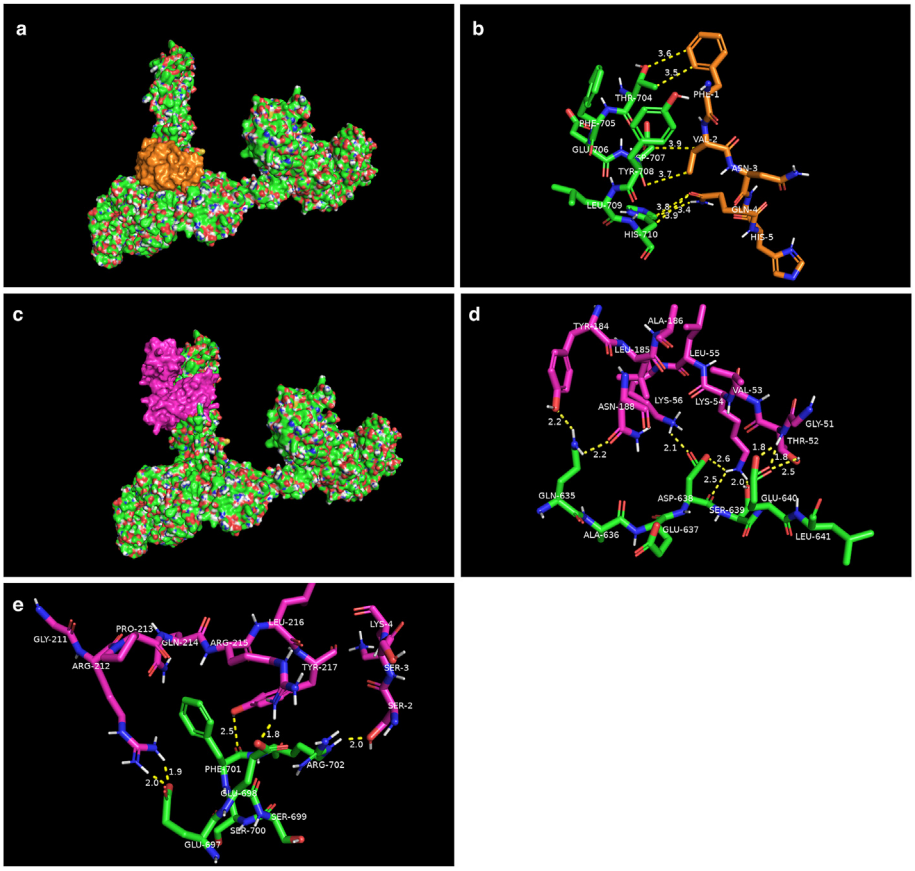

Figure 1. *In silico* binding between ribosomal protein L10a (RpL10a) and the insulin receptor (InR). The interaction between *Fm*-RpL10a and human InR was predicted using the PIPER programme on the ClusPro 2.0 server. (a) The 3D structure of InR protein (green) bound to insulin (orange). (b) The binding site between InR (green) and insulin (orange) at residues 704–710. (c) The binding of InR (green) with *Fm*-RpL10a protein (pink) derived by the PIPER programme on the ClusPro 2.0 server. (d) Binding between InR (green) and *Fm*-RpL10a (pink) at residues 635–640 of InR. (e) Binding between InR (green) and *Fm*-RpL10a (pink) at residues 697–702 of InR.

glucose utilisation in both healthy cells and IRCs. Stimulation with *Fm*-His-RpL10a increased glucose utilisation by both healthy cells and IRCs compared with the findings for unstimulated cells (Figure 7a–b). The result indicated after 12 and 24 h of stimulation, 1 μg/ml *Fm*-His-RpL10a, a minimal concentration, induced glucose utilization by IRCs compared with the findings in unstimulated IRCs (Figure 7b), whereas differences in glucose utilisation were only observed in healthy cells stimulated with ≥5 μg/ml *Fm*-His-RpL10a (Figure 7a) (independent-samples *t*-test, $P < 0.05$), indicating that *Fm*-RpL10a more readily induced glucose utilisation by IRCs than by healthy cells.

3.3. *Fm*-RpL10a changes the expression of glucose metabolism-related genes

This study, we focused on the effect of *Fm*-RpL10a on the glycolysis and gluconeogenesis. The glycolysis and gluconeogenesis genes in IRCs treated with 1 μg/ml *Fm*-His-RpL10a were changed (Figure 8). The expression of *Hk1*, which converts glucose to glucose-6-phosphate (G6K), was up-regulated. Conversely, *G6pc3* encoding G6Pase, which participates in gluconeogenesis, was down-regulated (Figure 8). In addition, *Pfk1*, which encodes phosphofructokinase-1, an enzyme that converts

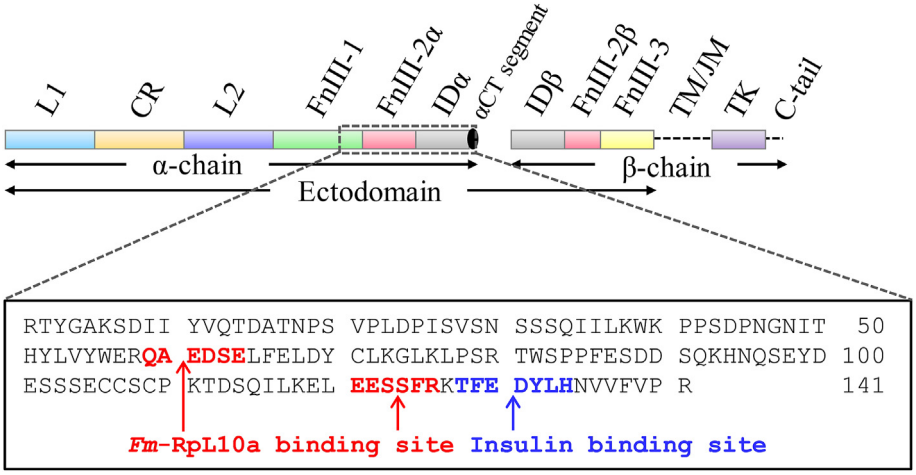

Figure 2. A linear schematic of the insulin receptor (InR) domains containing insulin binding sites and *Fm*-RpL10a binding site. The ribosomal protein L10a (RpL10a) and insulin binding sites located in the FnIII2 domain of InR and were shown in red and blue alphabets, respectively in the InR. The protein homology of the *C. griseus* InR target cloning site was in the square box.

Figure 3. The protein sequence alignment among cloning region (at amino acid residues 666-746, shown in black) of the insulin receptor (InR) from the *C. griseus*, full-length InR from *C. griseus* and *Homo sapiens*. Red squares indicate the amino acid sequences at the *Fm*-RpL10a binding site. The *C. griseus*'s InR target cloning site showed displayed 100% homology with the two full-length InRs.

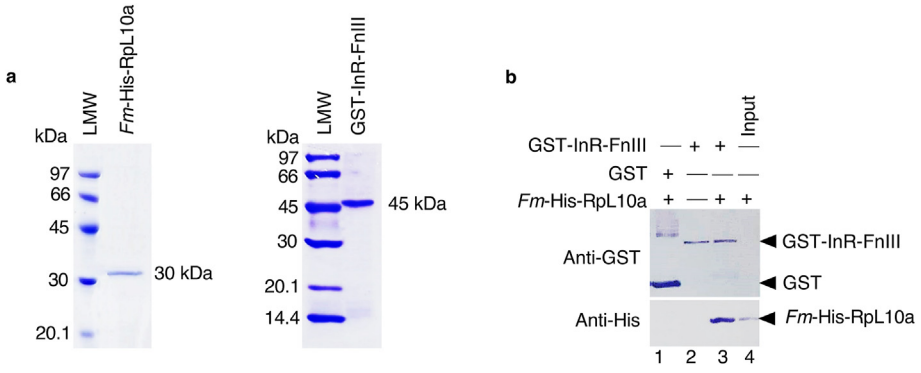

Figure 4. Pull down assay between ribosomal protein L10a (*Fm*-His-RpL10a, prey) and insulin receptor FnIII2 domain (InR-FnIII2,bait). (a) Coomassie blue staining of purified *Fm*-His-RpL10a and GST-InR-FnIII2. The proteins were separated using 12% SDS-PAGE. The molecular masses of *Fm*-His-RpL10a and GST-InR-FnIII2 were 30 and 45 kDa, respectively. (b) The interaction between *Fm*-His-RpL10a (prey) and GST-InR-FnIII2 (bait). The reaction mixtures contained GST incubated with *Fm*-His-RpL10a and GST-InR-FnIII2 incubated with and without *Fm*-His-RpL10a were pulled down with Glutathione Sepharose beads and detected via Western blotting using rabbit antibody-conjugated alkaline phosphatase. The original images were shown in Fig. S1 and S2.

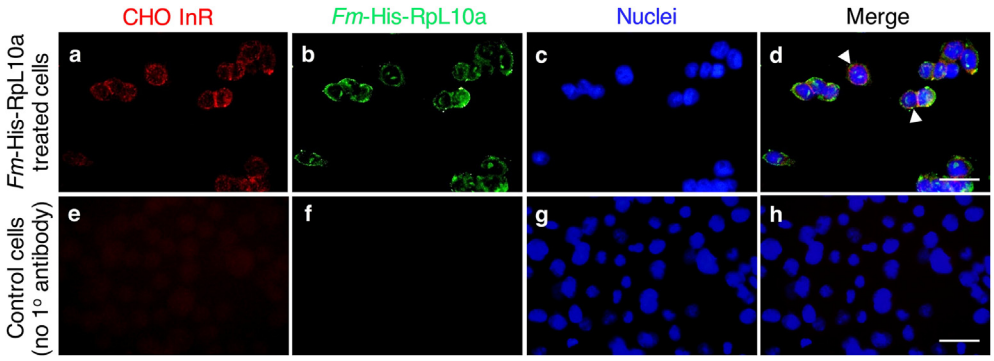

Figure 5. An immunofluorescence assay of the interaction between ribosomal protein L10a (*Fm*-His-RpL10a) and the insulin receptor (InR). Chinese hamster ovary (CHO–S) cells were incubated with 3 μg/ml *Fm*-His-RpL10a and probed with the antibody against a histidine tag and InR. (a: Red) CHO InR protein was stained with rhodamine, (b: green) *Fm*-His-RpL10a was stained with FITC and (c: blue) nuclei were stained with DAPI. The composite image (d) revealed that *Fm*-His-RpL10a could bind with CHO InR (arrowheads). Panels e–h present the immunofluorescence signal in the control group, in which no primary antibody was used for probing. The scale bar is 25 μm.

fructose 6-phosphate to fructose 1, 6-bisphosphate, was up-regulated (Figure 8). These changes in gene expression resulted in increased glycolysis and decreased gluconeogenesis (Figure 9), suggesting that *Fm*-RpL10a could induce absorption and sugar catabolism.

4. Discussion

The extracellular portion of InR consists of an α-chain, 194 residues of the β-chain, which contains six domains (L1, CR, L2, FnIII1, FnIII2 and FnIII3), and an inserted domain (ID) that lies within FnIII2 (Croll et al., 2016; Menting et al., 2013). The other portion of the β-chain acts as a transmembrane portion and cytoplasmic domain containing tyrosine kinase activity (Lawrence et al., 2007). Usually, insulin binds to the InR α-subunit at two binding sites, including low-affinity site 1 located in the L1 and CR domains of the receptor and high-affinity site 2 in the L2 and FnIII2 domains (De Meyts, 2008; Ward and Lawrence, 2009). This binding induces a conformation change in the two β-subunits of InR, leading to the phosphorylation of several intracellular substrates, including IRS1–4, SHC and other signaling intermediates (Taniguchi et al., 2006). In the present study, the interaction of *Fm*-RpL10a and InR was demonstrated via *in silico* analysis and confirmed via *in vitro* binding assays, including pull-down and immunofluorescence assays. The two *Fm*-RpL10a–binding sites in the FnIII2 domain of InR were located at residues 635–640 and 697–702. These binding site differ from the high-affinity binding site for insulin in InR (residues 704–710). The *in silico* binding analysis revealed that insulin interacts with InR at Thr704,

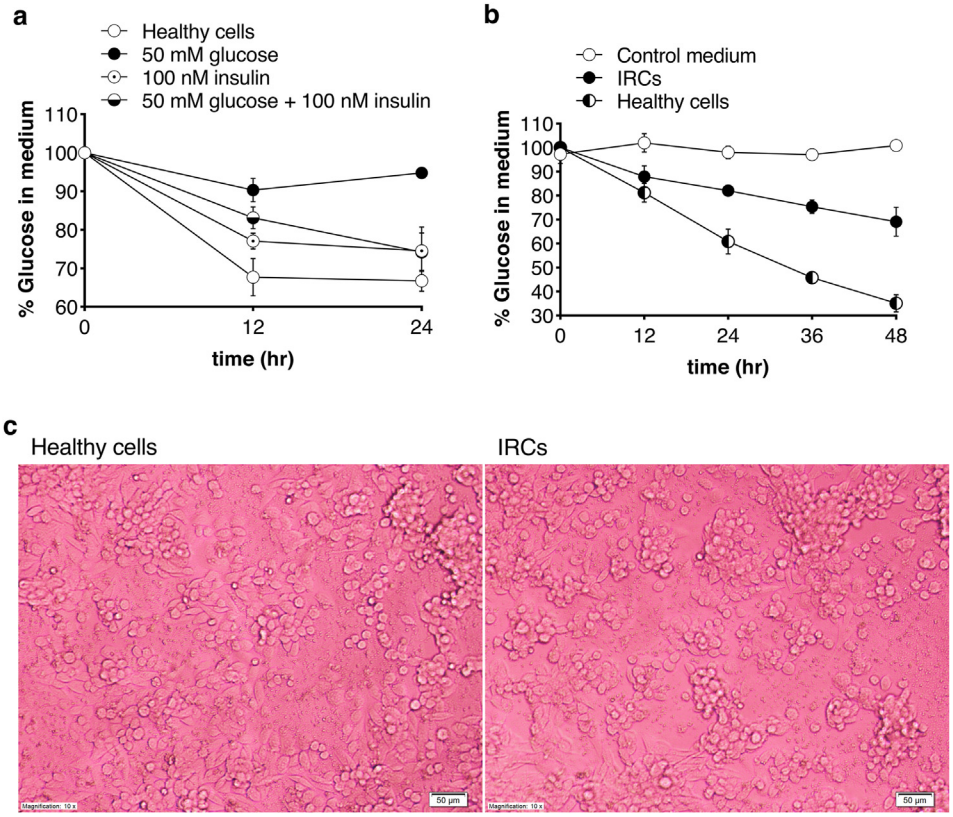

Figure 6. Insulin resistance in Chinese hamster ovary (CHO–S) cells. (a) The usage of glucose in the medium by CHO–S cells in which insulin resistance was induced under three conditions, including high (50 mM) glucose, high (100 nM) insulin and both high glucose and insulin, all utilising 24 h of induction. (b) The rate of glucose utilisation by high glucose-induced insulin-resistant cells (IRCs) compared with healthy cells over 48 h of induction. The medium was used as a negative control (c) Healthy cells and IRCs after 48 h of induction. The scale bar is 25 μm.

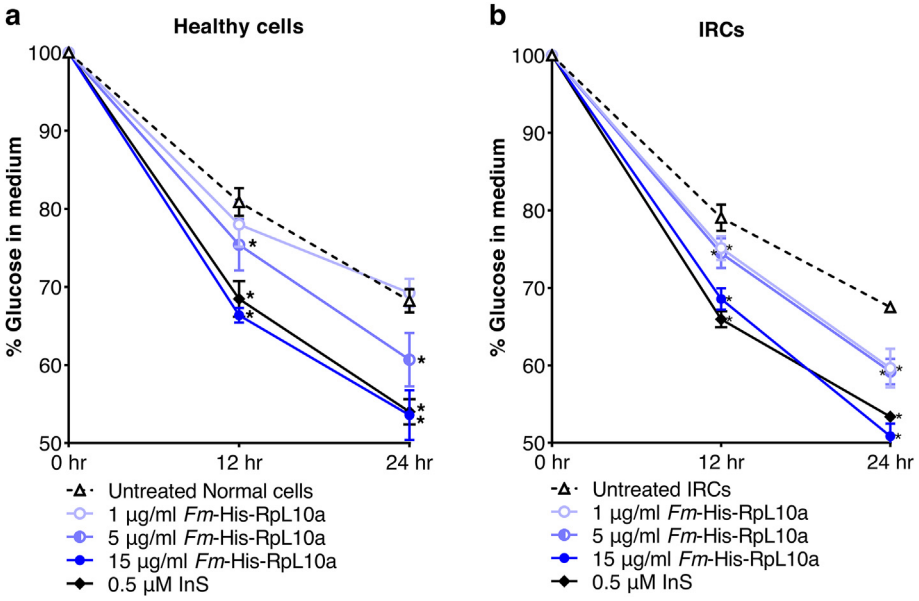

Figure 7. *Fm*-His-RpL10a protein induces glucose utilisation by both healthy cells and insulin-resistant cells (IRCs). IRCs and healthy cells were incubated with various concentrations of recombinant *Fm*-His-RpL10a. The rates of reduction of glucose utilisation by (a) healthy cells and (b) IRCs were determined during *Fm*-His-RpL10a stimulation compared with the findings in untreated cells. Cells incubated with 0.5 μM insulin were used as a control group. Each group was examined in triplicate. The statistical data were analysed using an independent-samples *t*-test. Asterisks indicate significant differences compared with untreated cells ($P < 0.05$).

Asp707 and His710. This result is similar to a previous finding that only His710 and His714 of InR are involved in its interaction with insulin (Menting et al., 2013) whereas *Fm*-RpL10a interacts with InR at Gln635, Asp638, Ser639, Glu640, Glu697, Glu698, Phe701 and Arg702. Thus, we suggest that *Fm*-RpL10a could bind to InR at a different region than insulin. Several reports indicated that many insulin mimetics regulated InR through different mechanisms. Some molecules activate InR via binding at the insulin binding site, such as 1, 2, 3, 4, 6-penta-O-galloyl-beta-D--glucopyranose (PGG), a component of tannic acid that acts as an anti-diabetic. PGG reduces blood glucose levels and improves glucose tolerance in diabetic and obese mice (Li et al., 2005). The chaetochromin derivative 4548-G05 induced glucose uptake in C2C12 myotubes by binding to InR at a different site than insulin (Qiang et al., 2014). In addition to the activation of InR phosphorylation and reduction of blood glucose levels through binding at the α subunit, some insulin mimetics can induce InR activity through binding to the β-subunits, such as the non-peptide molecule L-783,281 (Zhang et al., 1999) and LK16998 (Manchem et al., 2001). In this study, we also investigated the effect of *Fm*-RpL10a on glucose metabolism in IRCs. We found that the utilisation of glucose increased in proportion to the concentration of *Fm*-His-RpL10a

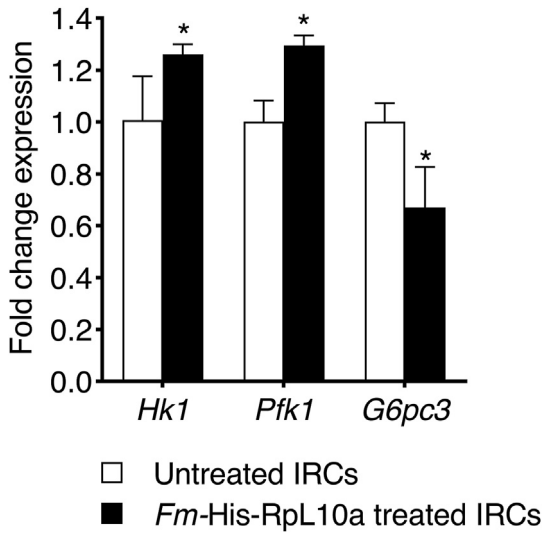

Figure 8. *Fm*-RpL10a alters the expression of glucose metabolism-related genes. Fold changes in the expression levels of *Hk1*, *Pfk1*, and *G6pc3* in IRCs treated with 1 μg/ml *Fm*-His-RpL10a for 24 h compared with their levels in untreated IRCs. The expression of each gene was normalised to that of the *β-actin* gene. The data were analysed for statistical significance using an independent-samples *t*-test. Error bars represent the mean ± SD, N = 3. Asterisks indicate significant differences ($P < 0.05$).

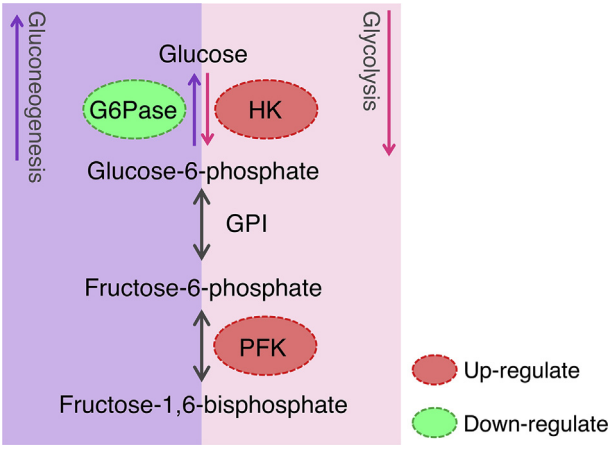

Figure 9. The diagram of glycolysis/gluconeogenesis partial pathway presents the expression of genes involved in glucose metabolism. Red indicates up-regulation, green indicates down-regulation.

in both IRCs and healthy cells. The *Fm*-His-RpL10a more strongly stimulated glucose utilisation in IRCs than in healthy cells. However, a usage of IRCs induced under high glucose condition, the excess of glucose also can induce the insulin independent glucose uptake via glucose transporter 1 (GLUT1) (Ebeling et al., 1998). In addition, insulin can also activate the insulin-like growth factor 1 receptor (IGF1R) and promote cell proliferation, although it is less extent than insulin-like growth factor 1 (IGF-1) (Boucher et al., 2010). While, RpL10a could induce cell proliferation by activating *InR* and *Shc* gene expression (Chaichanit et al., 2018; Wonglapsuwan et al., 2010). These evidences indicated that the proliferation of cell also affects the glucose utilisation. Therefore, it is essential to control cell number after insulin/RpL10a stimulation for further glucose utilisation experiment. In addition, the qRT-PCR data revealed that after *Fm*-His-RpL10a stimulation in IRCs, *Hk1* encoded a key enzyme in glycolysis was up-regulated, whereas *G6pc3* encoded a gluconeogenesis key enzyme was down-regulated.

Therefore, we suggest that the interaction between *Fm*-RpL10a and InR can stimulate insulin signaling together with glucose metabolism. However, transportation mechanism of the glucose after the *Fm*-RpL10a and InR interaction should be investigated. Since the study *in vitro* has a limitation on safety for further apply in human so and the *Fm*-RpL10a should be examined in diabetic animal models to confirm its potential application and safety for human use as an insulin mimetic in the future.

Declarations

Author contribution statement

Netnapa Chaichanit: Conceived and designed the experiments; Performed the experiments; Analyzed and interpreted the data; Wrote the paper.

Uraipan Saetan: Analyzed and interpreted the data.

Monwadee Wonglapsuwan: Performed the experiments; Analyzed and interpreted the data.

Wilaiwan Chotigeat: Conceived and designed the experiments; Performed the experiments; Analyzed and interpreted the data; Contributed reagents, materials, analysis tools or data; Wrote the paper.

Funding statement

This work was supported by the Royal Golden Jubilee Graduate Programme of the Thailand Research Fund (TRF), Thailand (4.JP.PS/56/B.1) and Thailand National Research Fund grant number SCI6201034S, Thailand.

Data availability statement

Data included in article/referenced in article.

Declaration of interests statement

The authors declare no conflict of interest.

Additional information

Supplementary content related to this article has been published online at https://doi.org/10.1016/j.heliyon.2020.e05714.

References

Babu, S., Krishnan, M., Rajagopal, P., Periyasamy, V., Veeraraghavan, V., Govindan, R., Jayaraman, S., 2020. Beta-sitosterol attenuates insulin resistance in adipose tissue via IRS-1/Akt mediated insulin signaling in high fat diet and sucrose induced type-2 diabetic rats. Eur. J. Pharmacol. 873, 173004.

Balcer-Kubiczek, E.K., Meltzer, S.J., Han, L.H., Zhang, X.F., Shi, Z.M., Harrison, G.H., Abraham, J.M., 1997. Csa-19, a radiation-responsive human gene, identified by an unbiased two-gel cDNA library screening method in human cancer cells. Oncogene 14, 3051–3057.

Belfiore, A., Frasca, F., Pandini, G., Sciacca, L., Vigneri, R., 2009. Insulin receptor isoforms and insulin receptor/insulin-like growth factor receptor hybrids in physiology and disease. Endocr. Rev.

Beutler, E., 1972. Disorders due to enzyme defects in the red blood cell. Adv. Metab. Disord.

Bluestone, J.A., Herold, K., Eisenbarth, G., 2010. Genetics, pathogenesis and clinical interventions in type 1 diabetes. Nature.

Boucher, J., Tseng, Y.H., Kahn, C.R., 2010. Insulin and insulin-like growth factor-1 receptors act as ligand-specific amplitude modulators of a common pathway regulating gene transcription. J. Biol. Chem. 285, 17235–17245.

Buranasin, P., Mizutani, K., Iwasaki, K., Pawaputanon Na Mahasarakham, C., Kido, D., Takeda, K., Izumi, Y., 2018. High glucose-induced oxidative stress impairs proliferation and migration of human gingival fibroblasts. PloS One 13, e0201855.

Campbell, R.K., 2009. Type 2 diabetes: where we are today: an overview of disease burden, current treatments, and treatment strategies. J. Am. Pharm. Assoc. 2003.

Chaichanit, N., Wonglapsuwan, M., Chotigeat, W., 2018. Ribosomal protein L10A and signaling pathway. Gene 674, 170–177.

Croll, T.I., Smith, B.J., Margetts, M.B., Whittaker, J., Weiss, M.A., Ward, C.W., Lawrence, M.C., 2016. Higher-resolution structure of the human insulin receptor ectodomain: multi-modal inclusion of the insert domain. Structure 24, 469–476.

De Meyts, P., 2008. The insulin receptor: a prototype for dimeric, allosteric membrane receptors? Trends Biochem. Sci.
Ebeling, P., Koistinen, H.A., Koivisto, V.A., 1998. Insulin-independent glucose transport regulates insulin sensitivity. FEBS Lett. 436, 301–303.
Fisicaro, N., Katerelos, M., Williams, J., Power, D., D'Apice, A., Pearse, M., 1995. Identification of genes downregulated in the thymus by cyclosporin-A: preliminary characterization of clone CSA-19. Mol. Immunol. 32, 565–572.
Lawrence, M.C., McKern, N.M., Ward, C.W., 2007. Insulin receptor structure and its implications for the IGF-1 receptor. Curr. Opin. Struct. Biol. 17, 699–705.
Lee, C.C., Hsu, W.H., Shen, S.R., Cheng, Y.H., Wu, S.C., 2012. Fagopyrum tataricum (Buckwheat) improved high-glucose-induced insulin resistance in mouse hepatocytes and diabetes in fructose-rich diet-induced mice. Exp. Diabetes Res. 2012.
Li, Y., Kim, J., Li, J., Liu, F., Liu, X., Himmeldirk, K., Ren, Y., Wagner, T.E., Chen, X., 2005. Natural anti-diabetic compound 1,2,3,4,6-penta-O-galloyl-D-glucopyranose binds to insulin receptor and activates insulin-mediated glucose transport signaling pathway. Biochem. Biophys. Res. Commun. 336, 430–437.
Livak, K.J., Schmittgen, T.D., 2001. Analysis of relative gene expression data using real-time quantitative PCR and the 2-ΔΔCT method. Methods 25, 402–408.
Manchem, V.P., Goldfine, I.D., Kohanski, R.A., Cristobal, C.P., Lum, R.T., Schow, S.R., Shi, S., Spevak, W.R., Laborde, E., Toavs, D.K., Villar, H.O., Wick, M.M., Kozlowski, M.R., 2001. A novel small molecule that directly sensitizes the insulin receptor in vitro and in vivo. Diabetes 50, 824–830.
Menting, J.G., Whittaker, J., Margetts, M.B., Whittaker, L.J., Kong, G.K.W., Smith, B.J., Watson, C.J., Žáková, L., Kletvíková, E., Jiráček, J., Chan, S.J., Steiner, D.F., Dodson, G.G., Brzozowski, A.M., Weiss, M.A., Ward, C.W., Lawrence, M.C., 2013. How insulin engages its primary binding site on the insulin receptor. Nature 493, 241–245.
Moura, L.F.W.G., da Silva Costa, H.P., da Silva Neto, J.X., Dias, L.P., Magalhães, F.E.A., van Tilburg, M.F., Florean, E.O.P.T., de Oliveira, J.T.A., de Oliveira Bezerra de Sousa, D., Guedes, M.I.F., 2020. Orally hypoglycemic activity of an insulin mimetic glycoprotein isolated from Cnidoscolus quercifolius Pohl. (Euphorbiaceae) seeds, Cq-IMP. Int. J. Biol. Macromol. 159, 886–895.
Nelson, B.A., Robinson, K.A., Buse, M.G., 2000. High glucose and glucosamine induce insulin resistance via different mechanisms in 3T3-L1 adipocytes. Diabetes 49, 981–991.
Nordlie, R.C., 1985. Fine tuning of blood glucose concentrations. Trends Biochem. Sci.
Palasin, K., Makkapan, W., Thongnoi, T., Chotigeat, W., 2014. Stimulation of ovarian development in white shrimp, Fenneropenaeus merguiensis De Man, with a recombinant ribosomal protein L10a. Aquaculture 432, 38–45.
Pende, M., Kozma, S.C., Jaquet, M., Oorschot, V., Burcelin, R., Le Marchand-Brustel, Y., Klumperman, J., Thorens, B., Thomas, G., 2000. Hypoinsulinaemia, glucose intolerance and diminished β-cell size in S6K1-deficient mice. Nature 408, 994–997.
Pritchett, T.L., McCall, K., 2012. Role of the insulin/Tor signaling network in starvation-induced programmed cell death in Drosophila oogenesis. Cell Death Differ. 19, 1069–1079.
Qiang, G., Xue, S., Yang, J.J., Du, G., Pang, X., Li, X., Goswami, D., Griffin, P.R., Ortlund, E.A., Chan, C.B., Ye, K., 2014. Identification of a small molecular insulin receptor agonist with potent antidiabetes activity. Diabetes 63, 1394–1409.
Robey, R.B., Hay, N., 2006. Mitochondrial hexokinases, novel mediators of the antiapoptotic effects of growth factors and Akt. Oncogene.
Saetan, U., Sangket, U., Deachamag, P., Chotigeat, W., 2016. Ovarian transcriptome analysis of vitellogenic and non-vitellogenic female banana shrimp (Fenneropenaeus merguiensis). PloS One 11, e0164724.
Schadt, E.E., Molony, C., Chudin, E., Hao, K., Yang, X., Lum, P.Y., Kasarskis, A., Zhang, B., Wang, S., Suver, C., Zhu, J., Millstein, J., Sieberts, S., Lamb, J., GuhaThakurta, D., Derry, J., Storey, J.D., Avila-Campillo, I., Kruger, M.J., Johnson, J.M., Rohl, C.A., van Nas, A., Mehrabian, M., Drake, T.A., Lusis, A.J., Smith, R.C., Guengerich, F.P., Strom, S.C., Schuetz, E., Rushmore, T.H., Ulrich, R., 2008. Mapping the genetic architecture of gene expression in human liver. PLoS Biol. 6, e107.
Seino, S., Bell, G.I., 1989. Alternative splicing of human insulin receptor messenger RNA. Biochem. Biophys. Res. Commun. 159, 312–316.
Shanik, M.H., Xu, Y., Krha, J.Š., Dankner, R., Zick, Y., Roth, J., 2008. Insulin Resistance and Hyperinsulinemia Is Hyperinsulinemia the Cart or the Horse?.
Taniguchi, C.M., Emanuelli, B., Kahn, C.R., 2006. Critical nodes in signalling pathways: insights into insulin action. Nat. Rev. Mol. Cell Biol.
Tremblay, F., Krebs, M., Dombrowski, L., Brehm, A., Bernroider, E., Roth, E., Nowotny, P., Waldhäusl, W., Marette, A., Roden, M., 2005. Overactivation of S6 kinase 1 as a cause of human insulin resistance during increased amino acid availability. Diabetes 54, 2674–2684.
Um, S.H., Frigerio, F., Watanabe, M., Picard, F., Joaquin, M., Sticker, M., Fumagalli, S., Allegrini, P.R., Kozma, S.C., Auwerx, J., Thomas, G., 2004. Absence of S6K1 protects against age- and diet-induced obesity while enhancing insulin sensitivity. Nature 431, 200–205.
Van Handel, E., 1985. Rapid determination of glycogen and sugars in mosquitoes. J. Am. Mosq. Contr. Assoc. 1, 299–301.
Ward, C.W., Lawrence, M.C., 2009. Ligand-induced activation of the insulin receptor: a multi-step process involving structural changes in both the ligand and the receptor. Bioessays 31, 422–434.
Wonglapsuwan, M., Chotigeat, W., Timmons, A., McCall, K., 2011. RpL10A regulates oogenesis progression in the banana prawn Fenneropenaeus merguiensis and Drosophila melanogaster. Gen. Comp. Endocrinol. 173, 356–363.
Wonglapsuwan, M., Miyazaki, T., Loongyai, W., Chotigeat, W., 2010. Characterization and biological activity of the ribosomal protein L10a of the white shrimp: Fenneropenaeus merguiensis De man during vitellogenesis. Mar. Biotechnol. 12, 230–240.
Xie, J., Wang, S., Ma, P., Ma, F., Li, J., Wang, W., Lu, F., Xiong, H., Gu, Y., Zhang, S., Xu, H., Yang, G., Lerner, R.A., 2020. Selection of small molecules that bind to and activate the insulin receptor from a DNA-encoded library of natural products. iScience 23, 101197.
Yoon, M.S., 2017. The role of mammalian target of rapamycin (mTOR) in insulin signaling. Nutrients.
Zhang, B., Salituro, G., Szalkowski, D., Li, Z., Zhang, Y., Royo, I., Vilella, D., Díez, M.T., Pelaez, F., Ruby, C., Kendall, R.L., Mao, X., Griffin, P., Calaycay, J., Zierath, J.R., Heck, J.V., Smith, R.G., Moller, D.E., 1999. Discovery of a small molecule insulin mimetic with antidiabetic activity in mice. Science (80-.) 284, 974–977.